EUROPEAN FUSION DEVELOPMENT AGREEMENT

EFDA–JET–CP(04)07-14

R.H. Goulding, F.W. Baity, F. Durodi, K.D. Freudenberg, J.C. Hosea, G.H. Jones, G.D. Loesser, P.U. Lamalle, I. Monakhov, B.E. Nelson, D.A. Rasmussen, D.O. Sparks, R. Walton, J.R. Wilson and JET EFDA Contributors

Results and Implications of the JET ITER-Like ICRF Antenna High Power Prototype Tests

Results and Implications of the JET ITER-Like ICRF Antenna High Power Prototype Tests

R.H. Goulding[1], F.W. Baity[1], F. Durodi [3], K.D. Freudenberg[1], J.C. Hosea[2], G.H. Jones[1], G.D. Loesser[2], P.U. Lamalle[3], I. Monakhov[4], B.E. Nelson[1], D.A. Rasmussen[1], D.O. Sparks[1], R. Walton[4], J.R. Wilson[2]
and JET EFDA Contributors*

[1]Oak Ridge National Laboratory, Oak Ridge, Tennessee, USA
[2]Princeton Plasma Physics Laboratory, Princeton, New Jersey, USA
[3]Association Euratom-Belgian State, LPP-ERM/KMS, Brussels, Belgium
[4]Association Euratom-UKAEA, Culham Science Centre, Abingdon, UK
** See annex of J. Pamela et al, "Overview of JET Results ",*
(Proc.20 [th] IAEA Fusion Energy Conference, Vilamoura, Portugal (2004).

Preprint of Paper to be submitted for publication in Proceedings of the
20th IAEA Conference,
(Vilamoura, Portugal 1-6 November 2004)

ABSTRACT.

A High Power Prototype (HPP) of the JET ITER-Like ICRF Antenna has been built and tested in a joint effort by ORNL, PPPL, ERM/KMS, and EFDA-JET. For the first time, high power vacuum tests have been performed on an antenna with features similar to those found in the current ITER antenna design. Advances include a new matching network using internal capacitors that is insensitive to target plasma characteristics, and increased power density to minimize the amount of port space required. Three-dimensional electromagnetic modeling has been used extensively to improve the antenna design and assist in interpretation of test results. During the HPP tests, capacitor voltages greater than 45 kV were achieved for short (0.05s) pulses. Voltages greater than 35 kV, approximately the voltage needed to couple the full 7.2MW design power into most JET plasmas, were sustained for moderate length (~0.5s) pulses. Long (10s) pulse operation was limited by excessive heating in localized regions due to rf dissipation, a problem that will be corrected in the final antenna. In this paper test results, associated numerical modeling, and their impact on the design of the final device will be reviewed.

1. INTRODUCTION

The JET ITER-Like Antenna High Power Prototype (HPP) was constructed to test to the greatest extent possible the performance of a new design for a high power, load tolerant Ion Cyclotron Range of Frequencies (ICRF) launcher, before production of a final version for JET [1]. Many aspects of HPP operation were tested, including (1) low power measurements of the tuning range, internal dissipation, tuning sensitivity, and cross coupling between straps, (2) high power, short pulse measurements of the antenna voltage limit and (3) long pulse measurements of the power limit. Tests of the HPP were highly successful to the extent that they demonstrated that the novel mechanical configuration could be successfully implemented, and that voltages equal to those required for the final JET ITER-Like antenna could be sustained on antenna structures for moderate length pulses. In addition, many 10 s pulses were run at a high enough power level to identify a small number of problems in the design that could have otherwise substantially limited the power handling of the final antenna. These problems involved arcing in regions of high electric field, and excessive power absorption due to high localized rf currents. Most of the novel features in the design have worked extremely well for the entire range of operating parameters that has been explored.

The design and testing phases of the HPP program coincided with our initial experience with a relatively new commercial 3-D RF design package, Microwave Studio (MWS) from Computer Simulation Technology [2]. Although we did not have the MWS code available for most of the HPP design work, it has been used subsequently to develop a better understanding of the nature of some of the problems encountered during the tests, and to help devise solutions. The experience gained as a result of the comparison between tests and modeling results indicates that this and similar codes will be very valuable for the design of future ICRF antennas. This work is discussed later in the paper.

As a result of the tests and modeling, suggestions for several design changes were submitted to the JET ITER-Like antenna design group. The HPP antenna is presently being modified so that some of these changes can be tested at ORNL prior to operation of the actual antenna.

The organization of the remainder of this paper is as follows. Section 2 discusses the novel features of the HPP design, and Section 3 contains a review of some low power and high power test results. Section 4 contains an analysis of the most important problem encountered during the tests, and the paper ends with a discussion and conclusions in section 5.

2. FEATURES OF THE HIGH POWER PROTOTYPE

Figure 1 shows the HPP ICRF antenna installed in the central vacuum chamber of the Radio Frequency Test Facility (RFTF) at ORNL. Figure 2 is a vertical section of the HPP. The device was designed to replicate as closely as possible the mechanical, geometrical, and electrical design of the upper left quadrant of the JET ITER-Like antenna. This quadrant consists of 2 current straps oriented poloidally, fed in a conjugate-tee arrangement [3] through parallel capacitors and a quarter-wave transformer (Fig.1). The novel features of the HPP can be seen in figs.1 and 2. Many are shared with the ITER-like launcher. They include:

- A “conjugate-tee” resonant circuit featuring internal vacuum matching capacitors, designed to maintain a voltage standing wave (VSWR) ratio below 1.5 for an order of magnitude change in plasma resistive loading
- Matching capacitors, manufactured by Comet, Ltd., having a unique, tritium compatible, triple bellows design allowing them to be connected in series between the current straps and quarter-wave transformer. Unlike previous antenna designs with internal capacitors [4], both ends are held above ground voltage and exposed to the chamber vacuum. The capacitors also have reinforced braze joints between the copper electrodes and alumina insulators, allowing them to withstand a factor of 6 higher bending stress than a standard Comet capacitor of comparable dimensions. Together with the vacuum window, these carry the full gravity and disruption loads associated with the inner conductor of the quarter-wave transformer.
- An integral, low impedance (9.3Ω) quarter-wave transformer to transform the desired 3Ω matching impedance to the JET transmission line impedance of 30Ω. The transformer has a large, racetrack shaped inner conductor with bolt-on covers and the capacitor actuation subsystem contained entirely within it.
- “Plug-in” flanges on the capacitors that allow the module, consisting of the quarter wave transformer and capacitors, to be easily replaced without requiring in-vessel entry. As a result, the fixed ends of the capacitors are not directly water cooled,
- Short, wide current straps to maximize power handling.

Some aspects of the HPP are different from the ITER-like antenna. Because it only replicates one quadrant of the latter, the current patterns in the region where the bottom current strap connects to the bottom of the surrounding “box” are different. Another difference is that a layer of “electroless” nickel is plated onto the surfaces of the current straps and feeds, with a second layer of electrolytic nickel plated above this in order to prevent outgassing. The ITERlike antenna current straps will

have only electrolytic plating. Also, the ITER-like antenna uses hydraulic actuators rather than the vacuum stepping motors used in the HPP to vary the capacitor tuning. There are several other minor differences that are not discussed here.

3. HPP TEST RESULTS

3.1 LOW POWER MEASUREMENTS

A large number of low power measurements have been made, including two-port scattering parameter measurements at the capacitor "plug-in" flanges [5], and synthesized Time-Domain Reflectometry (TDR) measurements to determine equivalent transmission line parameters for the current straps and feeds. Matching curves have been obtained, and studies of the sensitivity of the antenna impedance match to the capacitor positions have been made. Due to space limitations, we will discuss only the matching sensitivity measurements here.

Figure 3 shows an example of a measurement of the matching sensitivity in vacuum. It shows contours of constant VSWR, measured with an Agilent 8753-C network analyzer, as a function of capacitance values for the upper and lower matching capacitors. The data for this graph was obtained from over 1000 measurements obtained by the control system as it automatically stepped the capacitors through a range of values around the previously determined match point. The data shown is for 50MHz, where the sensitivity to the capacitance value is near the maximum. The sensitivity measurement indicates a required precision of 0.5 pF to obtain a Voltage Standing Wave Ratio (VSWR) < 1.5. This corresponds to ~100 micron accuracy in the position of the capacitor variable electrode. An accuracy of 20 microns is needed to obtain a VSWR near 1.0. This information has been used to determine specifications for the hydraulic capacitor actuators that will be installed on the actual antenna.

3.2 HIGH POWER TESTS

The first goal of the high power tests was to determine the antenna voltage limit. The antenna was prepared for these tests by baking for 16 hours at ~150^{o}C, and by multipactor conditioning, which has been discussed previously [5]. During short pulse tests at 50MHz a maximum voltage of ~ 46 kV was achieved on both capacitors, after a problem resulting from arcing between the private limiter tiles and Faraday shield rods was resolved by temporarily removing the tiles. No arcing was observed at the voltage limit. It may have been possible to reach higher voltages, but the test was stopped at this point because the value achieved was 4kV higher than the voltage required to couple 2MW of power to the nominal JET resistive plasma load of 2Ω /m. Figure 4 shows example voltage traces with maximum capacitor voltages > 46kV, taken on two separate shots. The input power in each case was ~300W.

When the pulse length was increased tenfold to ~0.5s, voltages of 36kV were achieved (fig.5). In this case, the voltage appeared to be limited by a rise in the background pressure, which occurred when the RF power was applied. Breakdown occurred when the pressure exceeded ~ 0.04Pa, as measured in the vacuum vessel surrounding the quarter-wave transformer. The pressure spikes

generally became larger as the input power was increased, but could also vary significantly between pulses at the same power.

The pulse length was then increased to 10s, the nominal pulse length for the JET ITER-like antenna. Figure 6 shows the highest voltages achieved for each capacitor for this pulse length. The data was again obtained from two different pulses. As in the case of the 0.5s pulses, the voltage and power were limited by pressure spikes. A series of these are shown in fig.7. The first spike above .01Pa occurs at the time of the first 10s pulse. In addition, bright glows were observed on the left hand side of the antenna box (looking from the front) near the top and bottom. They occurred in the region of the "flexipivot" sidewall, which consists of thin, parallel Inconel 718 plates. Each is 2mm thick, with a 2mm gap between them. This structure provides compliance for the thermal expansion of the Faraday shield elements (fig.2), which are made of beryllium in the actual antenna. Figure 8 shows the antenna box and current straps. The front plate of the flexipivot is shown in fig.9, which is a close up of the region inside the white rectangle (fig.8) with the strap removed. An infrared image obtained at the end of a 10s pulse shows temperatures at the base of the flexipivot well above 250^{o}C (fig 10, white arrow). A post-operation inspection of the region shows that a small portion of the flexipivot melted (fig. 11), indicating that the temperature in this region exceeded 1290 ^{o}C.

4. ANALYSIS

The most serious problem revealed by the HPP test program was the flexipivot damage shown in fig.11. Since the end of tests, simulations have been performed to determine the origin of the melting. The method used has been to create a slightly simplified model of thelower half of the antenna in MWS. The model was then used to determine surface currents on all antenna structures, and exported to the ANSYS [6] commercial engineering package in order to run thermal simulations. Figure 12 a,b shows the result of MWS calculation of current density for 50MHz operation. The arrows indicate the direction of the rf current, with the size and color of the arrows indicating the magnitude of the current. It can be seen that there is a large current component flowing between the strap and the flexipivot, which bunches up at the base of the flexipivot where it is attached to the antenna box. This is precisely the region where melting was observed after the long pulse tests. It was expected that current flowing through the strap would return to the feed, which is located at the back of the box, by the shortest possible route, and that this current would be mostly separate from the image current in the flexipivot. This clearly did not turn out to be the case.

Figure 13 shows temperature contours calculated using ANSYS for the same current distribution. The result corresponds to the end of a 10s pulse at a power level of 80 kW, which is the power used for the long pulse tests. The maximum temperature in the entire structure occurs in the region where the melting was observed, although in the model it reached a maximum of only ~300^{o}C. Reasons for this discrepancy are being investigated. A solution to the overheating problem, which was determined with the help of MWS, was to add triangular plates at the top and bottom of the box to redistribute the current and reduce the maximum current density. The top plate was added to

correct a similar but less severe problem at the top of the box. The change in the current distribution with the bottom plate added is shown in fig.14 (a,b). Figure 15 shows the temperature contours for this case. The flexipivot now remains cool. There is a hot spot at the base of the triangular plate, but it is smaller in size, and the temperature rise is 20% smaller, than that observed on the flexipivot without the plate. The plate will be nickel plated to further limit the temperature excursion.

DISCUSSION AND CONCLUSIONS

In addition to the flexipivot damage, small cracks were observed on the sides of the current straps. As seen in figures 13 and 15, these are also regions where the temperature increases significantly during a pulse. It is believed that the cracking was caused by the presence of phosphorus in the electroless nickel plating, but the sidewalls of the straps have also been thickened in the design of the actual antenna to lower the temperatures in these regions by increasing the thermal mass.

The HPP tests provided important data that has been used to improve the design of the JET ITER-like antenna and increase its performance. Further HPP operation will take place in the coming year to test some of the design modifications. The MWS package, which is an example of the latest generation of 3-D electromagnetic modeling software, has proven very useful to the HPP work. Of course, computer models have been used for some time to improve the design of ICRF antennas. However, it has not been possible until now, using available resources, to achieve the level of detail required to replicate the electrical behavior of structures like the HPP antenna box and flexipivot. In the case of the HPP, the bulk of the modeling was done after the device itself was constructed. In the case of future antennas, it will be possible to fully examine an antenna concept and eliminate most regions where excessive electric fields or current densities exist early in the design process.

REFERENCES

[1]. Durodié, F. et al., "The ITER-like ICRH Launcher Project for JET", (15th Topical Conference on Radio Frequency Power in Plasmas, Moran, Wyoming, 2003) AIP Conf. Proc. **694**, American Institute of Physics, Melville, N.Y. (2003), pp. 98-101.

[2]. http://www.cst.de/

[3]. Lamalle, P.U. et al., "Radio-Frequency Matching Studies for the JET ITER-like ICRF System", (15th Topical Conference on Radio Frequency Power in Plasmas, Moran, Wyoming, 2003) AIP Conf. Proc. **694**, American Institute of Physics, Melville, N.Y. (2003), pp. 118-121.

[4]. Hoffman, D. H. et al., "The design of high-power ICRF antennas for TFTR and Tore Supra", (7th Topical Conference on Radio Frequency Power in Plasmas, Kissimmee, Florida, 1987) AIP Conf. Proc. **159**, American Institute of Physics, Melville, N.Y. (1987), pp. 302-305.

[5]. Goulding, R. H. et al., "Initial operation of the JET ITER-like high power prototype ICRF antenna", (15th Topical Conference on Radio Frequency Power in Plasmas, Moran, Wyoming, 2003) AIP Conf. Proc. **694**, American Institute of Physics, Melville, N.Y. (2003), pp. 102-5.

[6]. http://www.ansys.com/

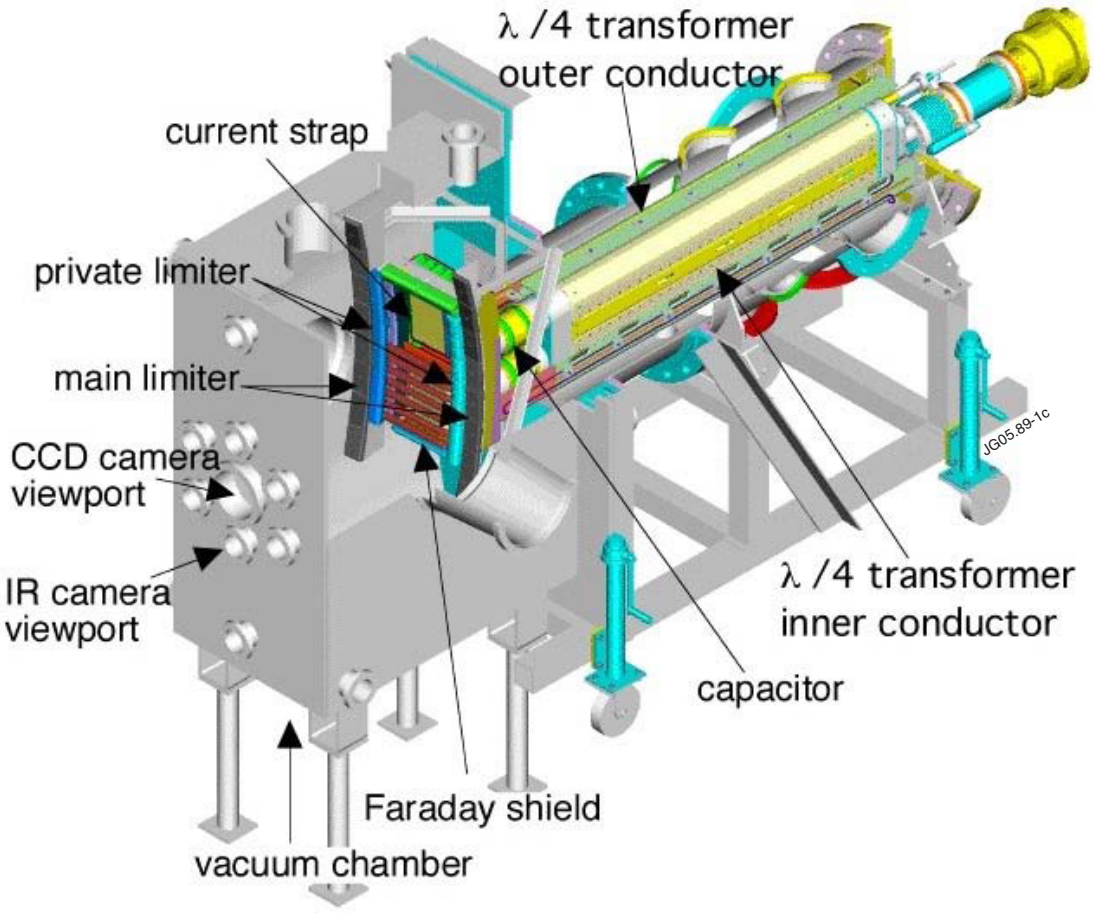

Figure 1: HPP Installed IN RFTF

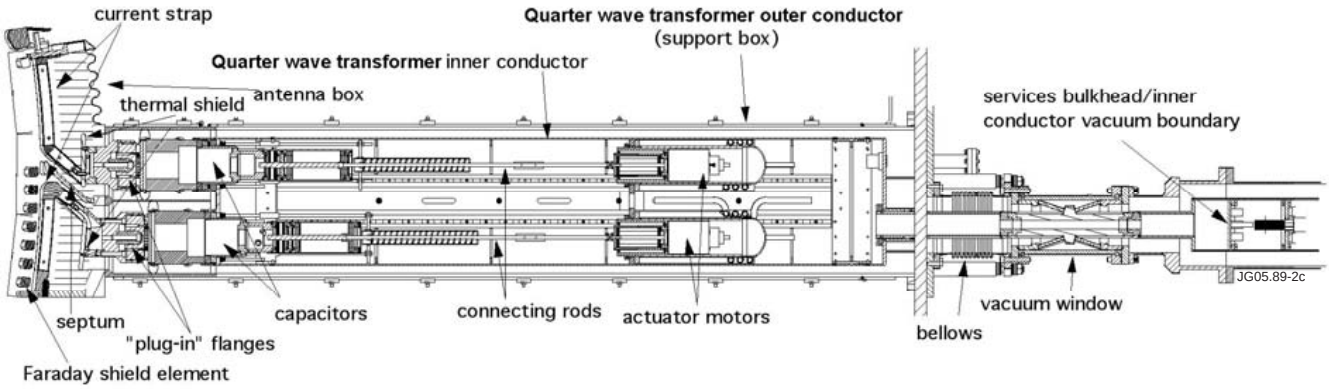

Figure 2: HPP Vertical section

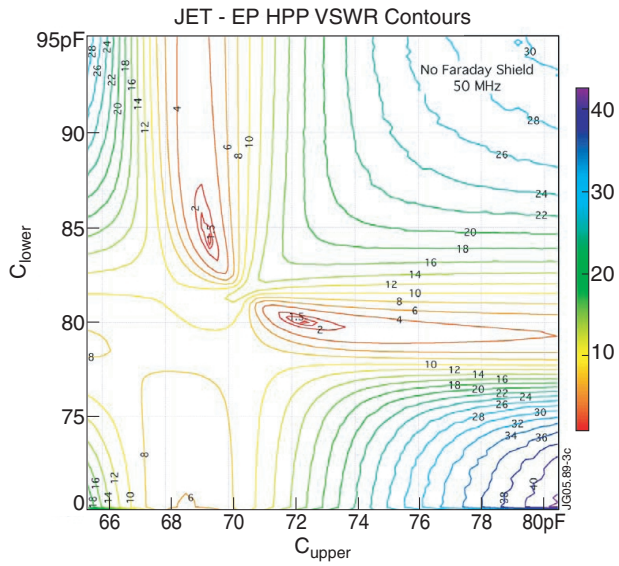

Figure 3: Sensitivity of matching to capacitance settings.

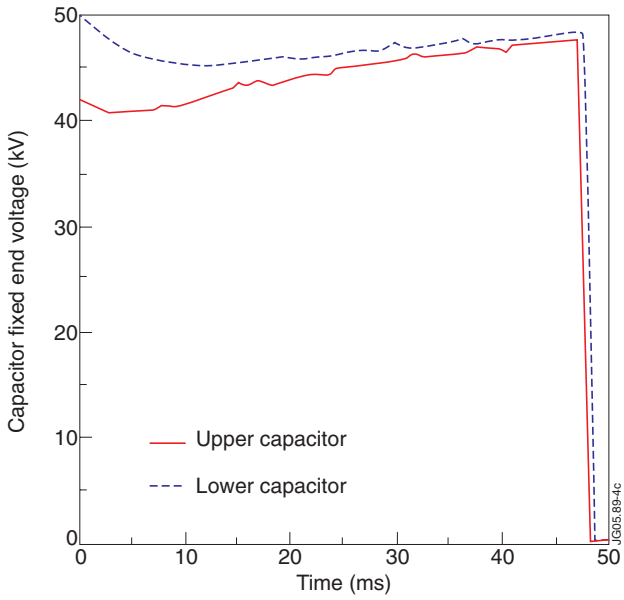

Figure 4: Highest voltages achieved in short pulse tests.

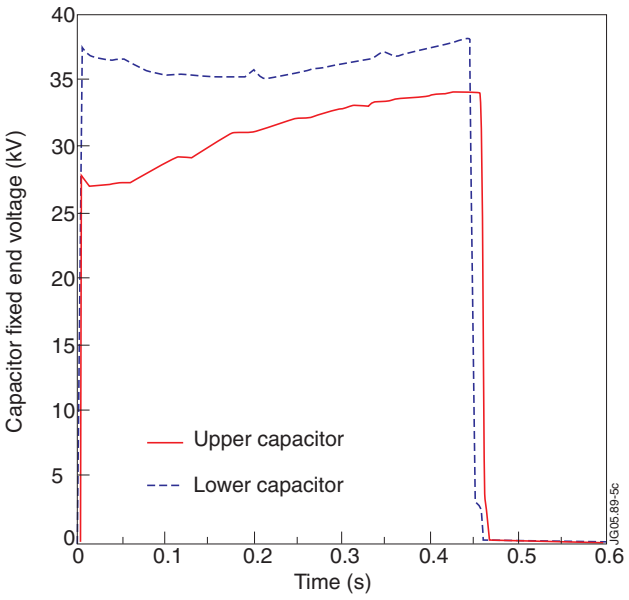

Figure 5: Highest voltages achieved for half second pulses.

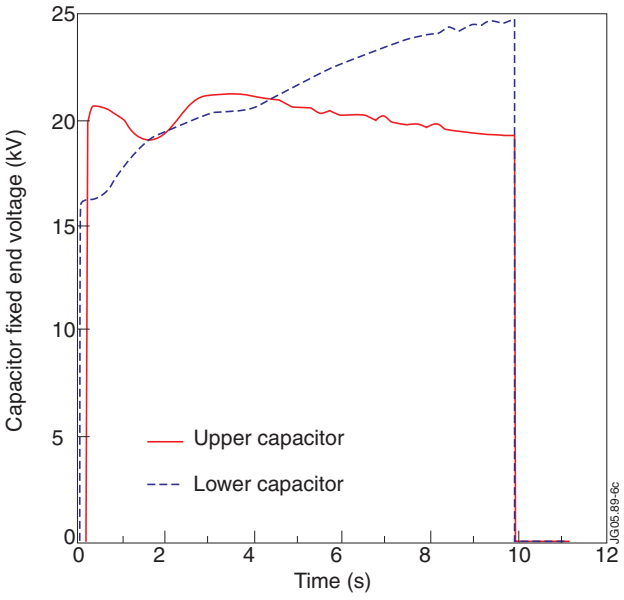

Figure 6: Highest voltages achieved durimg 10s pulses.

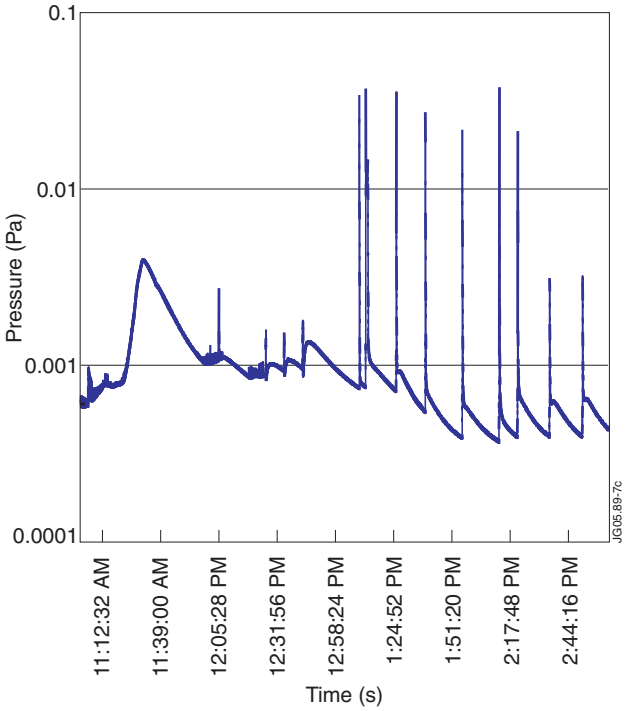

Figure 7: Pressure versus time during long pulses series.

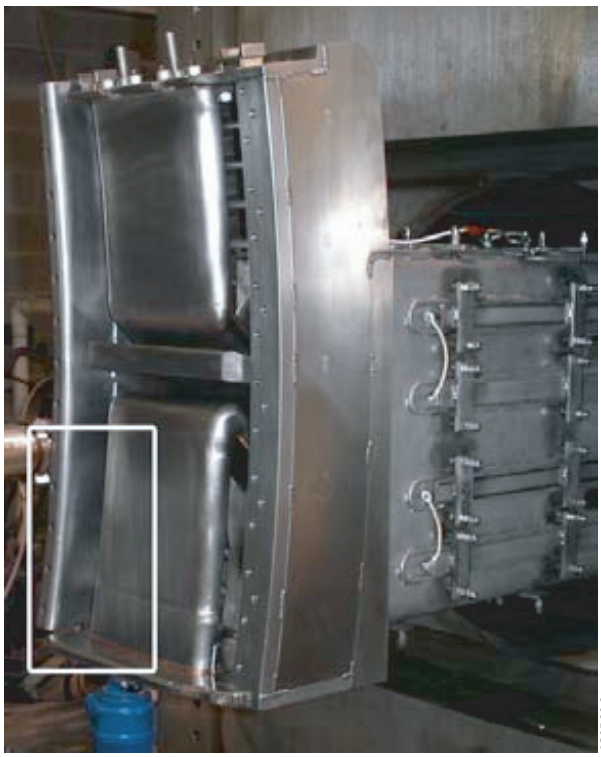

Figure 8: Antenna box and current straps.

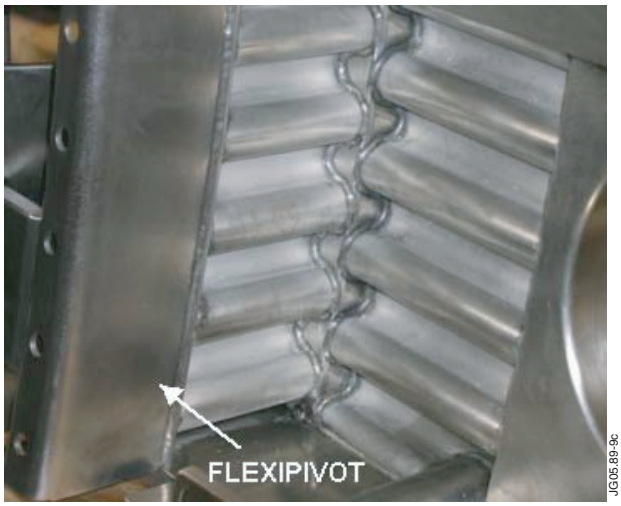

Figure 9: Portion of flexipivot and antenna box.

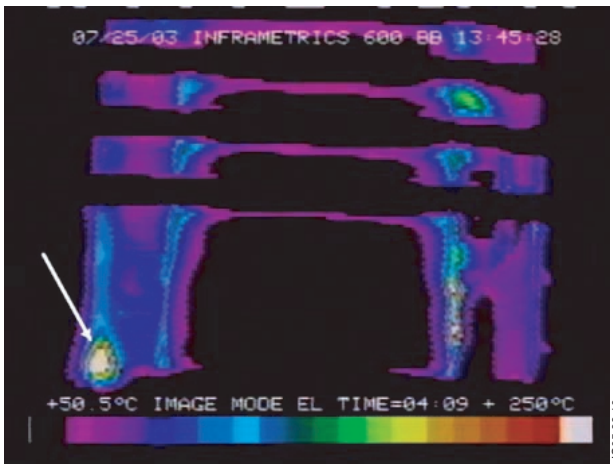

Figure 10: IR temperature measurement of bottom strap and antenna box.

Figure 11: Bottom of flexipivot showing melted region.

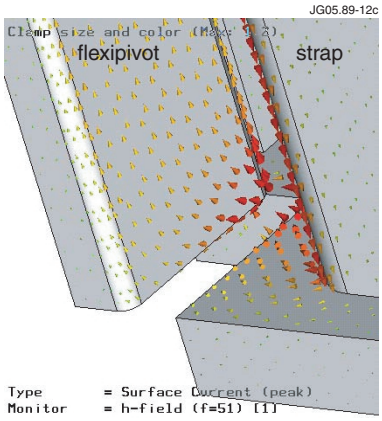

Figure 12 (a): Current density front view.

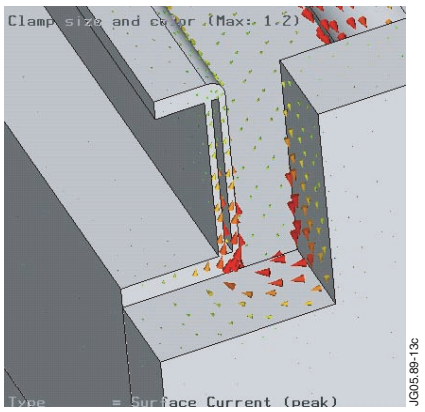

Figure 12 (b): Current density bottom view.

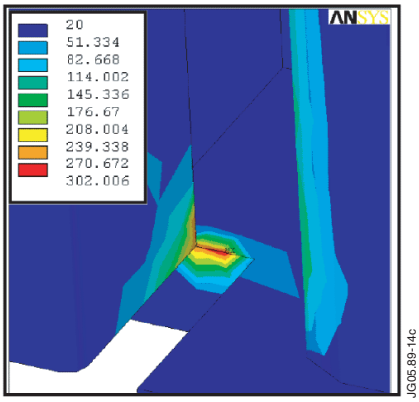

Figure 13: Flexipivot/box temperatures.

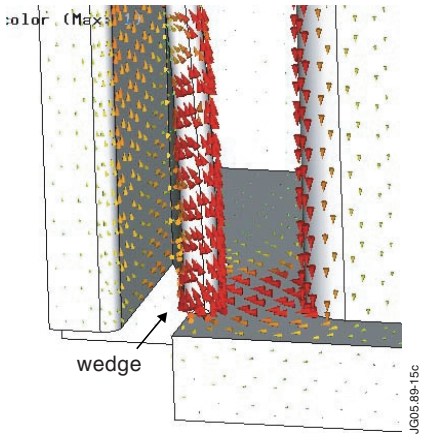

Figure 14(a): Current density with wedge.

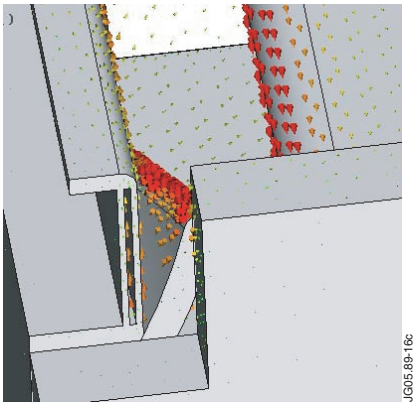

Figure 14(b): Current density with wedge bottom view.

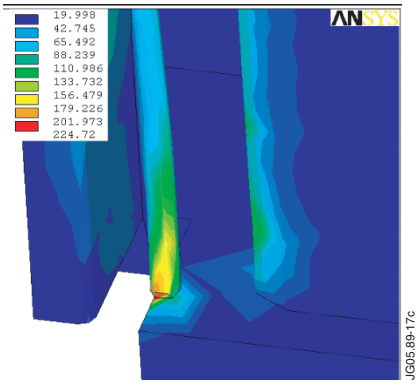

Figure 15: Temperature contours with wedge.